

Generalized Zero Shot Learning For Medical Image Classification

Dwarikanath Mahapatra¹

¹Inception Institute of Artificial Intelligence, UAE

dwarikanath.mahapatra@inceptioniai.org

Abstract

In many real world medical image classification settings we do not have access to samples of all possible disease classes, while a robust system is expected to give high performance in recognizing novel test data. We propose a generalized zero shot learning (GZSL) method that uses self supervised learning (SSL) for: 1) selecting anchor vectors of different disease classes; and 2) training a feature generator. Our approach does not require class attribute vectors which are available for natural images but not for medical images. SSL ensures that the anchor vectors are representative of each class. SSL is also used to generate synthetic features of unseen classes. Using a simpler architecture, our method matches a state of the art SSL based GZSL method for natural images and outperforms all methods for medical images. Our method is adaptable enough to accommodate class attribute vectors when they are available for natural images.

1. Introduction

Medical image classification is an important step in computer aided diagnosis. In the present era, deep learning methods have achieved state of the art results for many medical image classification tasks such as diabetic retinopathy grading [31, 112, 38, 25, 181, 59, 49, 123, 39, 15, 110], digital pathology image classification [55, 29, 10, 12, 84, 73, 193, 151, 99, 70, 54, 69, 115, 94] and chest xray images [35, 185, 95, 116, 119, 66, 65, 68, 129, 64, 145, 143, 142, 60, 57], to name a few. Fully supervised learning (FSL) methods that achieve state of the art results have access to disease classes (labels) in the training and test sets. However in many real-world scenarios we may not have access to samples of all possible diseases. A common scenario is the diagnosis of radiological images, such as chest xrays. Unseen classes are generally classified into one of the seen classes, resulting in wrong diagnosis and treatment planning. For deployment in clinical settings it is essential that a machine learning model learns to recognize novel test cases.

Zero shot learning (ZSL) aims to learn plausible rep-

resentations of unseen classes from labeled data of seen classes, and recognize unseen classes during test time. In a more generalized setting we expect to encounter both seen and unseen classes during the test phase, and a reliable model should accurately predict both classes. This is a case of generalized zero shot learning (GZSL) which is a challenging scenario since we do not want to predict unseen classes as one of the seen classes. We propose a GZSL method for medical image classification using self supervised learning (SSL), demonstrate its effectiveness across different datasets and also shows its applicability to natural images.

GZSL has been a widely explored topic for natural images [27, 182, 190, 85, 158, 177, 121, 86, 40, 180, 89, 11, 87, 47, 16, 191, 109, 92, 114] where seen and unseen classes are characterized by class attribute vectors. A model learns to correlate between class attribute vectors and corresponding feature representations. This gives a strong reference point in synthesizing features of both seen and unseen classes, since by inputting the class attribute vector of the desired class the corresponding feature representation can be generated. However medical images do not have such well defined class attributes since it requires high clinical expertise and time to define unambiguous attribute vectors for different disease classes. Hence it is not a straightforward task to apply state of the art GZSL methods to medical image classification. While this makes GZSL for medical images a challenging task, it is nevertheless essential to tackle this problem due to the potentially immense benefit.

Initial approaches to tackle ZSL [21, 188, 172, 173, 81, 174, 91, 165, 163, 179, 176, 71, 126, 175, 125, 192, 98, 97, 96, 122, 150, 51] learnt cross-modal relationships between visual feature and semantic embeddings (class attribute vectors). Subsequently, recent generative approaches to GZSL [189, 27, 118, 169, 171, 117, 131, 168, 67, 93, 149, 147, 148, 146, 61, 63, 183, 62], used generative adversarial networks (GANs) to optimize the divergence between the data distribution of seen classes and generated features. Consequently, generators trained on seen class features cannot accurately represent unseen classes. The sub-optimal synthetic data does not lead to high performance of such mod-

els. As an attempt to circumvent this problem some methods [160, 153, 58, 144, 138, 140, 141, 139, 135, 136, 130, 127, 137, 152, 124] utilize unlabeled data of unseen classes in a transductive way. However they require two GANs for seen and unseen classes as they do not consider the relations between source and target domains.

However, methods leveraging transductive approaches are particularly relevant for medical classification tasks [186, 111, 120, 26, 24, 134, 79, 78, 48, 77, 46, 36, 37, 14, 90, 76, 88, 166, 13, 74, 75, 108, 83, 50]. Absence of any supervised information from the unseen domain makes it very challenging to differentiate between disease labels, especially when many labels show similar appearance to the untrained eye. In our method we also leverage the unlabeled data of unseen classes as a guidance to train our GZSL method.

Another tricky issue facing GZSL applications in general and medical images in particular is the potentially large semantic gap between images of different classes. Consequently synthesizing such unseen class features from the seen classes can be challenging. Leveraging unlabeled unseen class data (e.g., using anchors) can be effective in bridging the semantic gap [186, 30, 132, 82, 72, 80, 8, 100, 101, 105, 7]. In an attempt to address the above challenges our paper makes the following contributions:

1. We propose a GZSL approach using self supervised learning (SSL) for medical image classification. Our method outperforms state of the art methods for multiple medical image datasets, and matches their performance on natural images.
2. We use SSL for: 1) deriving anchor vectors through **improved** clustering; and 2) feature synthesis of seen and unseen classes.
3. We achieve GZSL of medical images without using class attribute vectors commonly used for natural images. This is important for real world clinical scenarios where defining class attribute vectors is a time consuming and expensive task.

2. Prior Work

(Generalized) Zero-Shot Learning: In Zero-Shot Learning [188, 104, 6, 106, 107, 103, 102, 128, 113, 28, 2, 133, 33, 164], the goal is to recognize classes not encountered during training. External information about the novel classes may be provided in forms of semantic attributes [52], visual descriptions [1], or word embeddings [155]. Zero-shot learning has been addressed using Generative Adversarial Networks (GANs) [189], Variational Autoencoders (VAE) [170] or both of them [190].

In generalized zero-shot learning (GZSL), the purpose is to recognize images from known and unknown domains.

Many works [27, 182, 170, 189, 190] obtain impressive results by training GANs in the known domain and generate unseen visual features from the semantic labels. This allows them to train a fully supervised classifier for two domains, which is robust to the biased recognition problem. The work by Huang et al. [34] describes a Generative Dual Adversarial Network (GDAN) which couples a Generator, a Regressor and a Discriminator. The interaction between the three components produces various visual features conditioned on class labels. Keshari et al. [43] use overcomplete distributions to generate features of the unseen classes, while Min et al. [156] use domain aware visual bias elimination for synthetic feature generation. Different from the above works we achieve GZSL without the need for descriptive class attribute vectors, but by specifying the class label of the desired output feature. GZSL for medical image tasks have seen limited applications such as registration [45] and artefact reduction [23].

Self-Supervised Learning: These methods consist of two main approaches; 1) pre-text tasks and 2) down-stream tasks. Solving pre-text tasks learns a proper data representation, although the task itself may not be relevant, while down-stream tasks are used to evaluate the quality of features learned by self-supervised learning and are independent of pre-text tasks. Contrastive learning approaches such as MoCo [32] and SimCLR [22] are popular and give state-of-the-art results for down-stream task-based methods. Self-supervised learning (SSL) also addresses labeled data shortage and has found wide use in medical image analysis by using innovative pre-text tasks for active learning [123], anomaly detection [11], data augmentation [87], semi-supervised histology classification [56], stain normalization [89] and registration [180]. Recent works also use self supervision for domain adaptation [167] and perhaps the first work to combine GZSL and SSL [186]. While our work is inspired from [186] in using SSL for GZSL, and using GANs for feature synthesis, there are significant differences such as: 1) we do not use class attribute vectors for training. Since medical images do not have defined class attribute vectors we use a simpler architecture for GZSL. 2) [186] use a single generator but two discriminators to differentiate between seen and unseen classes. However we make use of a single generator and one discriminator to differentiate between all classes by leveraging anchor vectors; 3) We use a SSL based clustering approach to derive the anchor vectors of each class, including unseen classes. We use high level knowledge of the number of classes as a supervisory signal.

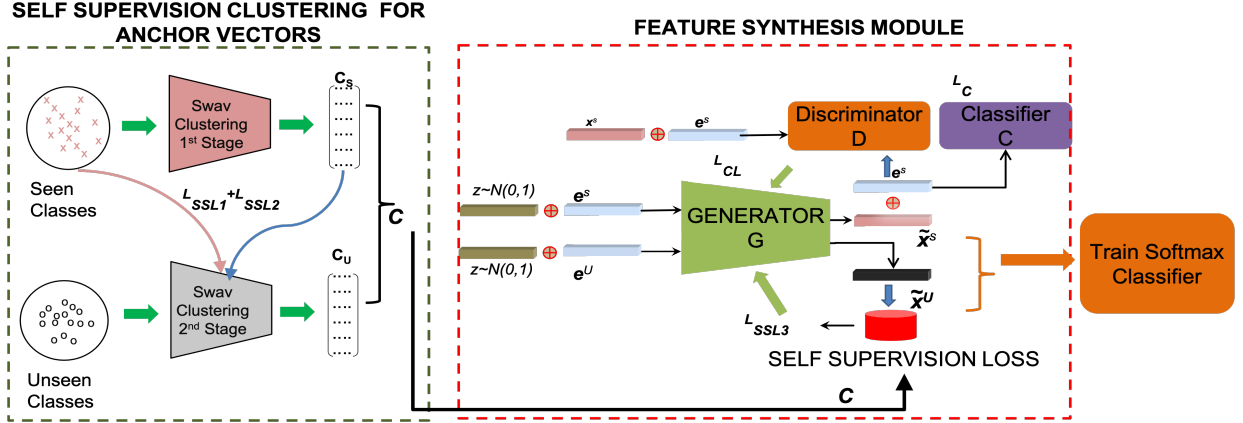


Figure 1. Architecture of proposed SC-GZSL method. In the first step we generate anchor vectors (cluster centroids) by using SSL within the SwAV clustering approach [20]. We have two clustering stages: one for Seen class samples and second for Unseen classes. Feature generation leverages one Generator and one Discriminator alongwith anchor vectors (from clustering) to derive SSL loss terms.

3. Method

3.1. Method Overview

Figure 1 depicts our proposed workflow. In the first step we generate anchor vectors (cluster centroids) by using SSL within the SwAV clustering approach [20]. We have two clustering stages: one for Seen class samples and second for Unseen classes. Anchor vectors of the Seen class samples are used to get SSL based loss terms for the second clustering stage. The second step involves feature generation that takes a noise vector and desired class label of output vector to synthesize features. Anchor vectors from the clustering stage are used to derive SSL based loss terms. Synthesized and real features of unseen and seen classes are used to train a softmax classifier for identifying different disease classes.

3.2. SSL Clustering To Obtain Anchor Vectors

Let the number of classes in the Seen set be n_S , and the number of classes in the Unseen set is n_U . We assume that the total number of classes is known. We learn anchor vectors of the different classes by using the SSL based online clustering approach SwAV (Swapping Assignments between multiple Views) [20], and introduce additional SSL inspired loss terms. Typical offline clustering methods [5, 19] alternate between cluster assignment and centroid update. Since they require multiple passes over the dataset, such methods are slow for online clustering. To overcome the high training time and inspired by contrastive instance learning [187], [20] enforce that different augmentations of the same image are mapped to the same cluster. Multiple image views are contrasted by comparing their cluster assignments instead of features.

We take the cluster centers to be class anchor vectors since they give a reliable representation of the corresponding class. We choose to compute the anchor vectors in

an online fashion since the number of unseen classes may change in a dynamic way depending upon the specific use case. Given image features x_t and x_s from two different transformations of the same image, we compute their cluster assignments q_t and q_s by computing the distance of the features to a set of K cluster centers c_1, \dots, c_K . A “swapped” prediction problem is solved with the following loss function:

$$\mathcal{L}(x_t, x_s) = \ell(x_t, q_s) + \ell(x_s, q_t) \quad (1)$$

where $\ell(x, q)$ measures the fit between features x and assignment q . Thus we compare features x_t and x_s using their intermediate cluster assignments q_t and q_s . If the two x 's capture same information, we can predict the cluster assignment from the other feature.

Online clustering: Given image I_n , it is transformed to I_{nt} using transformation t from a set T of image transformations. A non-linear mapping f_θ transforms I_{nt} to a feature vector which is projected to the unit sphere, i.e., $x_{nt} = f_\theta(x_{nt}) / \|f_\theta(x_{nt})\|_2$. The cluster assignment q_{nt} is computed by determining the distance of x_{nt} to the set of cluster centroids, c_1, \dots, c_K . C denotes a matrix whose columns are c_1, \dots, c_k .

Swapped prediction problem: Each term in Eq.1 represents the cross entropy loss between q and the probability obtained by taking a softmax of the dot products of x_i and all columns in C , i.e.,

$$\ell(x_t, q_s) = - \sum_k q_s^{(k)} \log p_t^{(k)}, \quad p_t^{(k)} = \frac{\exp \frac{x_t^\top c_k}{\tau}}{\sum_{k'} \exp \frac{x_t^\top c_{k'}}{\tau}} \quad (2)$$

where $\tau = 0.1$ is the temperature parameter [187]. Computing this loss over all images and augmentations results

in the following loss function for swapped prediction:

$$\mathcal{L}(x_t, x_s) = -\frac{1}{N} \sum_{n=1}^N \sum_{s,t \sim T} \left[\frac{x_{nt}^\top C q_{ns}}{\tau} + \frac{x_{ns}^\top C q_{nt}}{\tau} \right] - \log \sum_{k=1}^K \exp\left(\frac{x_{nt}^\top c_k}{\tau}\right) - \log \sum_{k=1}^K \exp\left(\frac{x_{ns}^\top c_k}{\tau}\right). \quad (3)$$

This loss function is jointly minimized with respect to the centroids in C and parameters θ of f_θ .

Computing the cluster assignments: The clustering assignments q are computed in an online fashion using image features within a batch. Since the centroids in C are used across different batches, SwAV clusters multiple instances to their appropriate clusters. Given feature vectors $X = [x_1, \dots, x_B]$, we map them to centroids $C = [c_1, \dots, c_K]$ using $Q = [q_1, \dots, q_B]$, and we optimize Q to maximize the similarity between X and C ,

$$\max_{Q \in \mathcal{Q}} \text{Tr}(Q^\top C^\top X) + \epsilon H(Q), \quad (4)$$

where H is the entropy function, $H(Q) = -\sum_{ij} Q_{ij} \log Q_{ij}$ and $\epsilon = 0.05$ controls smoothness of mapping. A high ϵ could potentially result in a trivial solution where all samples collapse into a unique representation and are assigned uniformly to all prototypes.

Our Novel Contribution: We use the concept of anchor vectors to bridge the gap between seen and unseen classes, which is determined by the following steps: Assuming we have n_S seen classes we first cluster the Seen class images into n_S clusters and obtain their centroids as $C_S = c_1, \dots, c_{n_S}$. In the next pass we compute the clusters $C_U = c_{n_S+1}, \dots, c_{n_S+n_U}$ of the n_U unseen classes using the following additional constraints:

1. The centroids in C_S do not change since they have been computed from the seen classes.
2. A self supervised constraint is added where the centroids of the unseen classes are forced to be different from the seen class centroids. This is done to account for the situation that some of the Unseen classes may be semantically close to one or more Seen classes. This may happen when images of different disease labels have very similar appearance which can be a common occurrence for radiological images. This condition is implemented using:

$$\mathcal{L}_{SSL1} = \min \left(\text{CoSim}(C_S^i, C_U^j), \sigma_1 \right) \quad (5)$$

Here $\sigma_1 = 0.15$ is a parameter that determines the semantic distance between the centroids, and CoSim denotes cosine similarity.

3. We add a second self supervised constraint that the similarity of seen class sample, x_s^i , with its corresponding class centroid C_S^i is higher than their similarity w.r.t all C_U^j . This is achieved by randomly selecting samples from the Seen class training set during minibatch training and computing the different cosine similarities. This constraint is implemented by

$$\mathcal{L}_{SSL2} = \max \left(\text{CoSim}(x_s^i, C_S^i) - \text{CoSim}(x_s^i, C_U^j), \sigma_2 \right) \forall j \quad (6)$$

$\sigma_2 = 0.25$ controls the minimum degree of semantic difference between different classes.

The final loss term for clustering the Unseen class samples is $\mathcal{L}_{Unseen} = \mathcal{L}(x_s, x_t) + \lambda_1 \mathcal{L}_{SSL1} - \lambda_2 \mathcal{L}_{SSL2}$, where $\mathcal{L}(x_s, x_t)$ is defined in Eqn. 3. $\lambda_1 = 1.1$, $\lambda_2 = 0.7$ are the weights. The ‘ $-\lambda_2 \mathcal{L}_{SSL2}$ ’ ensures that the loss term does not increase arbitrarily which is possible for ‘ $+\lambda_2 \mathcal{L}_{SSL2}$ ’.

3.3. Feature Generation Network

Given the training images of Seen classes and unlabeled images of the Unseen classes we learn a generator $G : \mathcal{E}, \mathcal{Z} \rightarrow \mathcal{X}$, which takes a class label vector $e^y \in \mathcal{E}$ and a Gaussian noise vector $z \in \mathcal{Z}$ as inputs, and generates a feature vector $\tilde{x} \in \mathcal{X}$. The discriminator $D : \mathcal{X}, \mathcal{E} \rightarrow [0, 1]$ takes a real feature x or synthetic feature \tilde{x} and corresponding class label vector e^y as input and determines whether the feature vector matches the class label vector. The generator G aims to fool D by producing features highly correlated with e^y using a Wasserstein adversarial loss[4]:

$$\mathcal{L}_{WGAN} = \min_G \max_D \mathbb{E}[D(x, e^y)] - \mathbb{E}[D(\tilde{x}, e^y)] - \lambda \mathbb{E}[(\|\nabla_{\tilde{x}} D(\tilde{x}, e^y)\|_2 - 1)^2] \quad (7)$$

where the third term is a gradient penalty term, and $\tilde{x} = \alpha x + (1 - \alpha)\tilde{x}$. $\alpha \sim U(0, 1)$ is sampled from a uniform distribution.

3.3.1 Self Supervised Loss From Anchor Vectors

The discriminator D is a classifier that determines whether the generated feature vector \tilde{x} belongs to one of the seen classes. Since the unseen classes are not labeled we do not have a data distribution for them and hence we use self supervision to determine whether the generated feature vector matches an unseen class. As the anchor vectors (i.e., the cluster centers) are fixed, we calculate the cosine distance between the generated vector \tilde{x} and the anchor vector corresponding to the desired class y , i.e.

$$\mathcal{L}_{SSL3} = 1 - \text{CoSim}(\tilde{x}, c_y) \quad (8)$$

If \tilde{x} truly represents the desired class y then the cosine similarity between \tilde{x} and the corresponding anchor vector c_y should be highest amongst all $K(=n_S+n_U)$ anchor vectors, and the corresponding loss is lowest.

3.3.2 Classifier Loss

We expect that \tilde{x}^s (synthesized feature vector for seen classes) are predicted correctly by a pre-trained classifier CL with a loss defined as below

$$\mathcal{L}_{CL} = -\mathbb{E}_{(\tilde{x}^s, y^s) \sim P_{\tilde{x}^s}} [\log P(y^s | \tilde{x}^s, \theta_{CL})] \quad (9)$$

where $P(y^s | \tilde{x}^s, \theta_{CL})$ is the classification probability and θ_{CL} denotes fixed parameters of the pre-trained classifier.

3.4. Training and Implementation

The final loss function is defined as

$$\mathcal{L} = \mathcal{L}_{WGAN} + \lambda_{CL}\mathcal{L}_{CL} + \lambda_3 L_{SSL3} \quad (10)$$

where λ_{CL}, λ_3 are weights that balance the contribution of the different terms. Once training is complete we specify the label of desired class and input a noise vector to G which synthesizes a new feature vector. We combine the synthesized target features of the unseen class \tilde{x}^u and real and synthetic features of seen class x^s, \tilde{x}^s to construct the training set. Then we train a softmax classifier by minimizing the negative log likelihood loss:

$$\min_{\theta} -\frac{1}{|\mathcal{X}|} \sum_{(x,y) \in (\mathcal{X}, \mathcal{Y})} \log P(y|x, \theta), \quad (11)$$

where $P(y|x, \theta) = \frac{\exp(\theta_y^T x)}{\sum_{j=1}^{|\mathcal{Y}|} \exp(\theta_j^T x)}$ is the classification probability and θ denotes classifier parameters. The final class prediction is by $f(x) = \arg \max_y P(y|x, \theta)$

Implementation Details: We show results for natural and medical images and compare with existing GZSL methods. Extending our method to natural images is straightforward where in we replace the class label vector e^y with the corresponding class attribute vectors. For feature extraction, similar to [188], we use a pre-trained ResNet-101 to extract 2048 dimensional CNN features for natural images. The generator (G) and discriminator (D) are all multilayer perceptrons. G has two hidden layers of 2000 and 1000 units respectively while the discriminator D is implemented with one hidden layer of 1000 hidden units. We choose Adam [44] as our optimizer, and the momentum is set to (0.9, 0.999). The values of loss term weights are $\lambda_{CL} = 0.6, \lambda_3 = 0.9$. Training the Swav Clustering algorithm takes 12 hours and the feature synthesis network for 50 epochs takes 17 hours, all on a single NVIDIA V100 GPU (32 GB RAM). PyTorch was used for all implementations.

3.5. Evaluation Protocol

The seen class S can have samples from 2 or more disease classes, and the unseen class U contains samples from the remaining classes. We use all possible combinations of labels in S and U . Following standard practice for GZSL, average class accuracies are calculated for two settings: 1) **S**: training is performed on synthesized samples of $S+U$ classes and test on S_{Te} . 2) **U**: training is performed on synthesized samples of $S+U$ classes and test on U . We also report the harmonic mean defined as

$$H = \frac{2 \times Acc_U \times Acc_S}{Acc_U + Acc_S} \quad (12)$$

where Acc_S and Acc_U denote the accuracy of images from seen (setting S) and unseen (setting U) classes respectively:

4. Experimental Results

4.1. Dataset Description

We demonstrate our method’s effectiveness on natural images and the following medical imaging datasets for classification tasks. Datasets with a minimum of 3 disease classes (excluding normal label) were chosen to highlight the performance of feature synthesis.

1. **CAMELYON17** dataset [17]: contains 1000 whole slide images (WSIs) with 5 slides per patient: 500 slides for training and 500 slides for test. Training set has annotations of 3 categories of lymph node metastasis: Macro (Metastases greater than 2.0 mm), Micro (metastasis greater than 0.2 mm or more than 200 cells, but smaller than 2.0 mm), and ITC (single tumor cells or a cluster of tumor cells smaller than 0.2mm or less than 200 cells). We extract 224×224 patches from the different slides and obtain 130,000 tumor patches and 200,000 normal patches. We take a pre-trained ResNet101 and finetune the last FC layer using the CAMELYON16 dataset [9], which is closely related but different from CAMELYON17. A baseline fully supervised learning (FSL) method is implemented¹ which is the top ranked in the leaderboard.
2. **NIH Chest Xray** Dataset: For lung disease classification we adopted the NIH ChestXray14 dataset [185] having 112,120 expert-annotated frontal-view X-rays from 30,805 unique patients and has 14 disease labels. Original images were resized to 224×224 . A pre-trained resnet-101 was finetuned using the CheXpert dataset [35] and the chosen baseline FSL was from [162].

¹<https://grand-challenge-public.s3.amazonaws.com/evaluation-supplementary/80/46fc579c-51f0-40c4-bd1a-7c28e8033f33/Camelyon17.pdf>

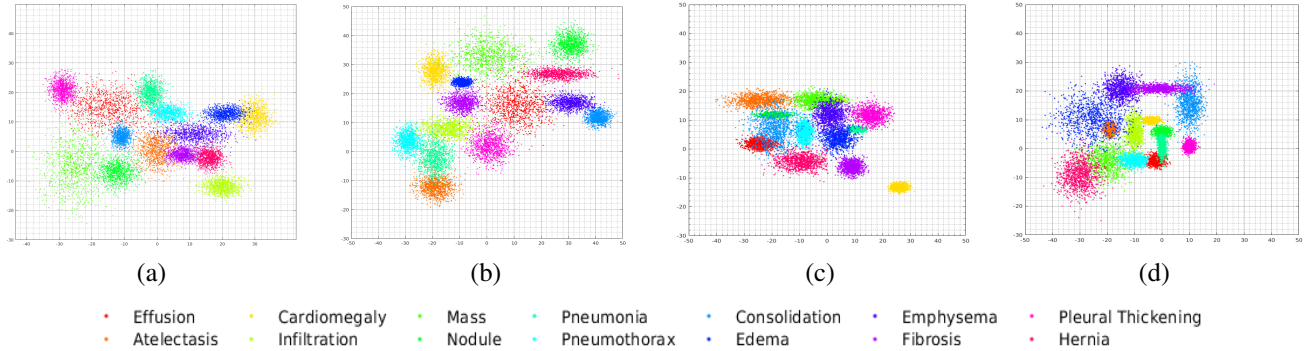


Figure 2. Feature visualizations for NIH ChestXray Dataset: (a) Seen+Unseen classes from actual dataset; distribution of synthetic samples generated by (b) SC-GZSL; (c) SC-GZSL_{w \mathcal{L}_{SSL3}} ; (d) SDGN [186]. Different colours represent different classes. (b) is closer to (a), while (c) and (d) are quite different.

3. **CheXpert Dataset:** We used the CheXpert dataset [35] consisting of 224,316 chest radiographs of 65,240 patients labeled for the presence of 14 common chest conditions. Original images were resized to 224×224 . A pre-trained resnet-101 was finetuned using the NIH dataset [185] and the baseline FSL method was of [161] which is ranked second for the dataset with shared code.
4. **Kaggle Diabetic Retinopathy dataset:** has approximately 35,000 images in the provided training set [41]. Images are labeled by a single clinician with the respective DR grade, out of 4 severity levels: 1- mild(2443 images), 2-moderate (5291 images), 3-severe (873 images), and 4-proliferative DR (708 images). The normal class 0 has 25810 images. A pre-trained resnet-101 was finetuned using [178] which has 9939 color fundus images (2720×2720) from 2740 diabetic patients. Although the number of classes are different from Kaggle the features are accurate since the end task is DR detection. The chosen baseline method was of [3]. Original images were resized to 224×224 .
5. **Gleason grading challenge dataset**² for prostate cancer (PCA) [42]. It has 333 Tissue Microarrays (TMAs) from 231 patients and has 5 Gleason grades. Six pathologists with 27, 15, 1, 24, 17, and 5 years of experience annotated the data and majority voting was used to construct the “ground truth label”. The training set had 200 TMAs while the validation set had 44 TMAs. A separate test set consisting of 87 TMAs from 60 other patients. Although a much larger dataset for PCA using WSIs is available³, the data cannot be used for external submissions⁴. The baseline FSL was the clas-

sification outcome of the top ranked method⁵. The feature extractor was a pre-trained ResNet101 finetuned using the CAMELYON16 dataset [9]. Since both are histopathology image datasets, the feature extractor is quite accurate. The high dimensional images were divided into 224×224 patches. The individual labels patches from normal images were all ‘normal’. For the diseased images (all Gleason grades except 1), the labels of individual patches were obtained using the multiple instance learning method of [18]. Thus we obtained more than 5,000 patches of each label.

Since we did not have labels of the organizer designated test sets of all datasets, a 70/10/20 split at patient level was done to get training, validation and test sets for NIH Chest Xray, CheXpert and Kaggle DR datasets.

For natural images we use the following five datasets: 1) CUB [184], Awa1 [52], Awa2 [188], SUN [159], and FLO [157]. CUB includes 11K images and 200 species of birds labeled with 312-D attributes. Awa1 and Awa2 consist of 50 kinds of animals described by 85-D attributes, containing 30K and 37K images respectively. SUN is a large-scale scene attribute dataset, including 717 classes and 14K images with 102-D attributes. FLO consists of 8K images from 102 flower classes. Adapting our method to natural images is done by replacing the class vector (e) with the class attribute vector.

4.2. Baseline Methods

We compare our method’s performance with the following GZSL methods employing different feature generation approaches such as CVAE or GANs: 1) CVAE based generation method of [34]; 2) over complete distribution (OCD) method of [43]; 3) self-supervised learning GZSL method of [186]; 4) FSL- Top performing FSL methods of cor-

²<https://gleason2019.grand-challenge.org/Home>

³<https://www.kaggle.com/c/prostate-cancer-grade-assessment/overview>

⁴<https://www.kaggle.com/c/prostate-cancer-grade->

<assessment/discussion/201117>

⁵<https://github.com/hubutui/Gleason>

responding datasets. Following GZSL protocol we report performance for Seen and Unseen classes. Our method is denoted as SC-GZSL (Selfsupervised Clustering based GZSL).

4.3. Visualization of Synthetic Image Features

Figure 2 (a) shows t-SNE plot of features from actual data from the NIH chest Xray dataset where the different classes are spread over a wide area, with slight overlap between some classes. Figure 2 (b) shows the distribution of synthetic features generated by our method. Although the corresponding clusters for the different classes have separate locations in the two figures they are similar to that of Figure 2 (a) in the sense that the different classes are similarly separated. Figure 2 (c) shows the feature distribution for our method without using self-supervision. The resulting distribution is compact without overlap between classes, which is not representative of the real-world case. Classifiers trained on such distributions perform poorly on unseen classes. Figure 2 (d) shows the feature distributions using SDGN [186]. Although it also uses SSL the resulting feature representation is less accurate than our proposed method which contributes to the corresponding inferior performance.

4.4. Generalized Zero Shot Learning Results

Table 1 summarizes the results of our algorithm on natural images. The best performing method amongst all competing methods is SDGN [186]. However we are able to outperform it despite using a much simpler architecture. A McNemar’s statistical test [154] shows that the results between SC-GZSL and SDGN is not very significant ($p = 0.062$), except for the SUN dataset ($p=0.01$). This dataset is particularly challenging as demonstrated by the fact that accuracy values are lower than other datasets.

The results for medical images shown in Table 2 shows our proposed method outperforms all competing GZSL methods including SDGN. This significant difference in performance can be explained by the fact that the complex architectures that worked for natural images will not be equally effective for medical images which have less information. Absence of attribute vectors for medical images is another contributing factor. The class attributes provide a rich source of information about natural images which can be leveraged using existing architectures. On the other hand medical images require a different approach.

4.5. Ablation Studies

Table 2 also shows results for the following ablation studies: 1) SCGZSL $_{w\mathcal{L}_{SSL1}}$ - SCGZSL without the loss term \mathcal{L}_{SSL1} (Eqn.5) for obtaining the anchor vectors, 2) SCGZSL $_{w\mathcal{L}_{SSL2}}$ - SCGZSL without the loss term \mathcal{L}_{SSL2} (Eqn.6) to get anchor vectors, 3) SCGZSL $_{\mathcal{L}}$ - Using only the

baseline loss term $\mathcal{L}(z_s, z_t)$ (Eqn.3) for clustering all seen and unseen classes together, and no \mathcal{L}_{SSL3} for feature synthesis; 4) SCGZSL $_{w\mathcal{L}_{SSL3}}$ - SCGZSL without the loss term \mathcal{L}_{SSL3} (Eqn.8) for training the feature synthesis network; 5) SCGZSL-only \mathcal{L}_{SSL3} - SCGZSL using only \mathcal{L}_{SSL3} for feature synthesis without $\mathcal{L}_{SSL1}, \mathcal{L}_{SSL2}$.

The first three ablation studies investigate the effect of clustering on the final classification results. Their significant performance degradation compared to SCGZSL indicates the importance of our novel SSL based terms ($\mathcal{L}_{SSL1}, \mathcal{L}_{SSL2}$) in obtaining accurate anchor vectors. The baseline method, SCGZSL $_{\mathcal{L}}$, does not use any form of self supervision and has lowest H values. Compared to SCGZSL, we observe that excluding \mathcal{L}_{SSL3} (SCGZSL $_{w\mathcal{L}_{SSL3}}$) leads to maximum reduction of H (more than 3.5%) across all datasets. This indicates that \mathcal{L}_{SSL3} makes the most significant contribution to our method’s performance. The use of anchor vectors makes it easier to synthesize features of unseen classes.

The influence of $\mathcal{L}_{SSL1}, \mathcal{L}_{SSL2}$ is quantitatively similar as shown by similar H values of SCGZSL $_{w\mathcal{L}_{SSL1}},$ SCGZSL $_{w\mathcal{L}_{SSL2}}$ across all datasets. However their difference in H values compared to SCGZSL is nearly 2.4% which is significant ($p = 0.01$). Thus the use of self supervision is an important factor in obtaining accurate anchor vectors (cluster centroids). Although the baseline clustering mechanism, SwAV, uses self supervision in the form of contrastive loss, including \mathcal{L}_{SSL1} and \mathcal{L}_{SSL2} significantly improves clustering accuracy. Excluding both $\mathcal{L}_{SSL1}, \mathcal{L}_{SSL2}$ and using the baseline SwAV (‘only $w\mathcal{L}_{SSL3}$ ’) gives significantly reduced H values for the different datasets despite using \mathcal{L}_{SSL3} for feature synthesis. This clearly indicates the importance of having accurate anchor vectors for our method. SCGZSL $_{\mathcal{L}}$ can be considered as the most basic method without using any of our proposed novel loss terms, and unsurprisingly gives the worst results.

4.6. Hyperparameter Selection

For all the competing methods in the case of medical images we start with the original values provided by the authors and vary them in range $x \pm 0.5x$ in steps of $x/10$, where x is the initial value. The best results are usually obtained using author provided values for each method.

Figure 3 (a) shows the harmonic mean values for the NIH Chest Xray dataset for different values of hyperparameters $\lambda_1, \lambda_2, \lambda_3$, while Figure 3 (b) shows the corresponding plots for different values of σ_1, σ_2 . The λ ’s were varied between [0.4 – 1.5] in steps of 0.05 and the performance on a separate test set of 10,000 images was monitored. We start with the base cost function of Eqn. 7, and first select the optimum value of λ_1 . λ_1 values is fixed and we then determine λ_2 , and then λ_3 by fixing λ_1, λ_2 . The order in which the parameters were set is important and we find the above

Method	Natural Images														
	CUB			AwA1			AwA2			SUN			FLO		
	S	U	H	S	U	H	S	U	H	S	U	H	S	U	H
f-Vaegan [190]	65.1	61.4	63.2	-	-	-	88.6	84.8	86.7	41.9	60.6	49.6	87.2	78.7	82.7
GXE [53]	68.7	57.0	62.3	89.0	87.7	88.4	90.0	80.2	84.8	58.1	45.4	51.0	-	-	-
SDGN [186]	70.2	69.9	70.1	88.1	87.3	87.7	89.3	88.8	89.1	46.0	62.0	52.8	91.4	78.3	84.4
GDAN [34]	66.7	39.3	49.5	-	-	-	67.5	32.1	43.5	89.9	38.1	53.4	-	-	-
OCD[43]	59.9	44.8	51.3	-	-	-	73.4	59.5	65.7	42.9	44.8	43.8	-	-	-
SCGZSL	71.7	70.6	71.1	88.5	88.1	88.3	89.9	89.3	89.6	50.3	62.1	55.6	91.8	79.4	85.2

Table 1. **GZSL Results For Natural Images:** Average per-class classification accuracy (%) and harmonic mean (H) accuracy of generalized zero-shot learning when test samples are from Seen(S) or Unseen (U) classes. Numbers for competing methods are taken from [186]. S, U denote Acc_S, Acc_U .

Method	Multiple Medical Image Datasets														
	CAMELYON17			NIH Xray			CheXpert			Kaggle DR			Gleason		
	S	U	H	S	U	H	S	U	H	S	U	H	S	U	H
f-VAEGAN [190]	90.2	88.2	89.2	82.9	80.0	81.4	88.5	87.6	88.0	92.8	90.2	91.5	88.2	85.1	86.6
GDAN [34]	91.1	89.1	90.1	83.8	80.9	82.3	89.2	88.0	88.6	94.2	91.0	92.6	88.8	86	87.4
OCD[43]	91.5	89.3	90.4	84.7	81.3	83.0	89.9	88.1	89.0	94.8	91.3	93.0	89.2	86.9	88
SDGN [186]	92.1	89.5	90.8	84.4	81.1	82.7	90.2	88.2	89.2	95.0	91.9	93.4	90.0	87.8	88.9
SCGZSL	93.5	91.1	92.3	87.2	84.3	85.7	91.8	89.4	90.6	96.1	93.2	94.7	92.1	89.5	90.8
FSL	93.7	93.5	93.6	87.4	86.9	87.1	92.1	92.5	92.3	96.4	96.1	96.2	92.4	92.2	92.3
SCGZSL	Ablation Studies														
$w\mathcal{L}_{SSL1}$	91.2	88.7	89.9	84.5	82.1	83.3	89.1	86.9	88.0	92.2	89.6	90.9	90.3	86.9	88.6
$w\mathcal{L}_{SSL2}$	90.8	88.1	89.4	84.0	82.2	83.1	88.8	86.2	87.5	91.8	88.2	90.0	89.2	86	87.6
$w\mathcal{L}_{SSL3}$	90.0	87.0	88.5	83.2	81.0	82.1	87.6	85.1	86.3	90.1	86.7	88.4	88.4	85.5	86.9
only \mathcal{L}_{SSL3}	89.3	86.4	87.8	82.6	80.7	81.6	87.0	84.5	85.7	88.9	85.9	87.4	87.7	84.9	86.3
\mathcal{L}	87.2	84.1	85.6	80.7	79.1	79.7	84.6	82.7	83.6	86.5	83.7	85.1	86.1	82.8	84.4

Table 2. **GZSL Results For Medical Images:** Average per-class classification accuracy (%) and harmonic mean accuracy of generalized zero-shot learning when test samples are from Seen (Setting S) or unseen (Setting U) classes. Results of ablation studies are also shown.

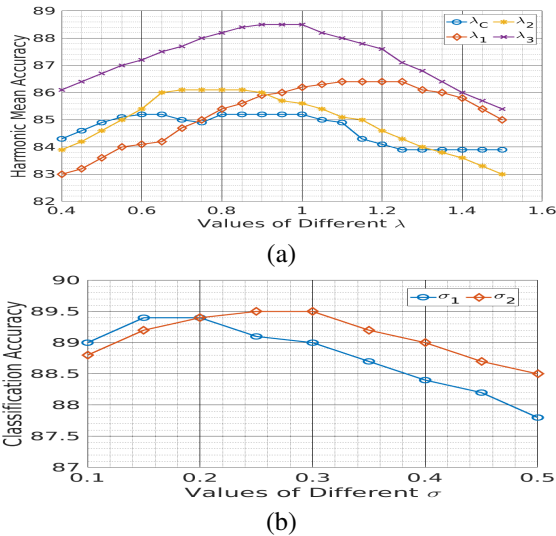


Figure 3. Hyperparameter Plots showing the value of H and classification accuracy for different values of: (a) λ ; (b) σ .

order as giving the best results. Similarly the value of σ 's were varied between [0.1, 0.5] in steps of 0.05, and the resulting classification accuracy of the Xray images was determined. i.e., whether they were assigned to the correct cluster (class).

Figure 4 shows, for the NIH Chest Xray and CAMELYON17 dataset, the effect of adding synthetic samples on Acc_S, Acc_U as a function of dataset augmentation factor. Increasing synthesized examples increases Acc_U at a high rate while reducing Acc_S , although at a lower rate. TSynthetic samples improve discriminative power of classifiers and reduce bias towards Seen classes.

5. Conclusion

We propose a GZSL approach for medical images without relying on class attribute vectors. Our novel method can accurately synthesize feature vectors of unseen classes by employing self supervised learning at different stages such as anchor vector selection, and training the feature generator. Using self supervision allows us to bridge the seman-

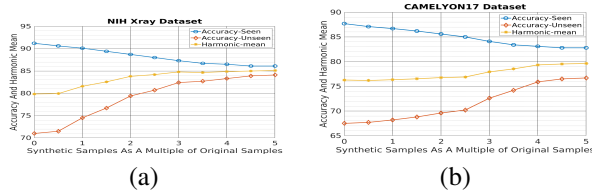


Figure 4. Value of accuracy and H when adding synthetic samples to the dataset: (a) NIH dataset; (b) CAMELYON17 dataset.

tic gap between Seen and Unseen classes. The distribution of synthetic features generated by our method are close to the actual distribution, while removing the self-supervised term results in unrealistic distributions. Experimental results show our method outperforms other GZSL approaches in literature.

References

- [1] Zeynep Akata, Scott Reed, Daniel Walter, Honglak Lee, and Bernt Schiele. Evaluation of output embeddings for fine-grained image classification. In *In Proc. IEEE CVPR*, pages 2927–2936, 2015. 2
- [2] BJ Antony, S Sedai, D Mahapatra, and R Garnavi. Real-time passive monitoring and assessment of pediatric eye health. In *US Patent App. 16/178,757*, 2020. 2
- [3] Teresa Araujo, Guilherme Aresta, Luís Mendonca, Susana Penas, Carolina Maia, Angela Carneiro, Ana Maria Mendonca, and Aurelio Campilho. DR—GRADUATE: uncertainty-aware deep learning-based diabetic retinopathy grading in eye fundus images. *Medical Image Analysis*, 2020. 6
- [4] Martin Arjovsky, Soumith Chintala, and Léon Bottou. Wasserstein gan. In *arXiv preprint arXiv:1701.07875*, 2017. 4
- [5] Yuki M. Asano, Christian Rupprecht, and Andrea Vedaldi. Self-labelling via simultaneous clustering and representation learning. In *International Conference on Learning Representations (ICLR)*, 2020. 3
- [6] P.R. Bastide, I.F. Kiral-Kornek, D. Mahapatra, S. Saha, A. Vishwanath, and S. Von Cavallar. Machine learned optimizing of health activity for participants during meeting times. In *US Patent App. 15/426,634*, 2018. 2
- [7] P.R. Bastide, I.F. Kiral-Kornek, D. Mahapatra, S. Saha, A. Vishwanath, and S. Von Cavallar. Visual health maintenance and improvement. In *US Patent 9,993,385*, 2018. 2
- [8] P.R. Bastide, I.F. Kiral-Kornek, D. Mahapatra, S. Saha, A. Vishwanath, and S. Von Cavallar. Crowdsourcing health improvements routes. In *US Patent App. 15/611,519*, 2019. 2
- [9] B. E. Bejnordi, M. Veta, P. J. van Diest, B. van Ginneken, N. Karssemeijer, G. Litjens, J. van der Laak, , and the CAMELYON16 Consortium. Diagnostic Assessment of Deep Learning Algorithms for Detection of Lymph Node Metastases in Women With Breast Cancer. *JAMA*, 318(22):2199–2210, 2017. 5, 6
- [10] B. Bozorgtabar, D. Mahapatra, and J-P. Thiran. Exprada: Adversarial domain adaptation for facial expression analysis. In *Press Pattern Recognition*, 100:15–28, 2020. 1
- [11] B. Bozorgtabar, D. Mahapatra, J.-P. Thiran, and L. Shao. SALAD: Self-supervised aggregation learning for anomaly detection on x-rays. In *In Proc. MICCAI*, pages 468–478, 2020. 1, 2
- [12] B. Bozorgtabar, D. Mahapatra, H. von Teng, A. Pollinger, L. Ebner, J-P. Thiran, and M. Reyes. Informative sample generation using class aware generative adversarial networks for classification of chest xrays. *Computer Vision and Image Understanding*, 184:57–65, 2019. 1
- [13] B. Bozorgtabar, D. Mahapatra, H. von Teng, A. Pollinger, L. Ebner, J-P. Thiran, and M. Reyes. Informative sample generation using class aware generative adversarial networks for classification of chest xrays. In *arXiv preprint arXiv:1904.10781*, 2019. 2
- [14] B. Bozorgtabar, D. Mahapatra, G. Vray, and J.-P. Thiran. Anomaly detection on x-rays using self-supervised aggregation learning. In *arXiv preprint arXiv:2010.09856*, 2020. 2
- [15] B. Bozorgtabar, D. Mahapatra, I. Zlobec, T.T. Rau, and J.P. Thiran. Computational pathology. *Frontiers in Medicine*, 7, 2020. 1
- [16] B. Bozorgtabar, M. Saeed Rad, D. Mahapatra, and J-P. Thiran. Syndemo: Synergistic deep feature alignment for joint learning of depth and ego-motion. In *In Proc. IEEE ICCV*, 2019. 1
- [17] P. Bándi, , and et al. From Detection of Individual Metastases to Classification of Lymph Node Status at the Patient Level: The CAMELYON17 Challenge. *IEEE Trans. Med. Imag.*, 38(2):550–560, 2019. 5
- [18] Gabriele Campanella, Vitor M.K. Silva, and Thomas J. Fuchs. Terabyte-scale deep multiple instance learning for classification and localization in pathology. In *arXiv preprint arXiv:1805.06983*, 2018. 6
- [19] Mathilde Caron, Piotr Bojanowski, Armand Joulin, and Matthijs Douze. Deep clustering for unsupervised learning of visual features. In *European Conference on Computer Vision*, 2018. 3
- [20] Mathilde Caron, Ishan Misra, Julien Mairal, Priya Goyal, Piotr Bojanowski, and Armand Joulin. Unsupervised learning of visual features by contrasting cluster assignments. In H. Larochelle, M. Ranzato, R. Hadsell, M. F. Balcan, and H. Lin, editors, *Advances in Neural Information Processing Systems*, volume 33, pages 9912–9924. Curran Associates, Inc., 2020. 3
- [21] Soravit Changpinyo, Wei-Lun Chao, Boqing Gong, and Fei Sha. Synthesized classifiers for zero-shot learning. In *2016 IEEE Conference on Computer Vision and Pattern Recognition (CVPR)*, pages 5327–5336, 2016. 1
- [22] T. Chen, S. Kornblith, M. Norouzi, and G. Hinton. A simple framework for contrastive learning of visual representations. In *arXiv preprint arXiv:2002.05709*, 2020. 2
- [23] Y. Chen, Y. Chang, S. Wen, Y. Shi, X. Xu, T. Ho, Q. Jia, M. Huang, and J. Zhuang. Zero-shot medical image artifact reduction. In *2020 IEEE 17th International Symposium on Biomedical Imaging (ISBI)*, pages 862–866, 2020. 2

- [24] Sourya Dipta Das, Saikat Dutta, Nisarg A Shah, Dwarikanath Mahapatra, and Zongyuan Ge. Anomaly detection in retinal images using multi-scale deep feature sparse coding. In *arXiv preprint arXiv:2201.11506*, 2022. **2**
- [25] K. Devika, Dwarikanath Mahapatra, Ramanathan Subramanian, and Venkata Ramana Murthy Oruganti. Outlier-based autism detection using longitudinal structural mri. *IEEE Access*, 10:27794–27808, 2022. **1**
- [26] K. Devika, Dwarikanath Mahapatra, Ramanathan Subramanian, and Venkata Ramana Murthy Oruganti. Outlier-based autism detection using longitudinal structural mri. In *arXiv preprint arXiv:2202.09988*, 2022. **2**
- [27] Rafael Felix, Vijay Kumar, Ian Reid, and Gustavo Carneiro. Multi-modal cycle-consistent generalized zero-shot learning. In *ECCV*, pages 21–37, 2018. **1, 2**
- [28] R Garnavi, D Mahapatra, PK Roy, and RB Tennakoon. System and method to teach and evaluate image grading performance using prior learned expert knowledge base. In *US Patent App. 10,657,838*, 2020. **2**
- [29] Z. Ge, D. Mahapatra, X. Chang, Z. Chen, L. Chi, and H. Lu. Improving multi-label chest x-ray disease diagnosis by exploiting disease and health labels dependencies. In *press Multimedia Tools and Application*, pages 1–14, 2019. **1**
- [30] Z. Ge, D. Mahapatra, S. Sedai, R. Garnavi, and R. Chakravorty. Chest x-rays classification: A multi-label and fine-grained problem. In *arXiv preprint arXiv:1807.07247*, 2018. **2**
- [31] Varun Gulshan, Lily Peng, Marc Coram, Martin C. Stumpe, Derek Wu, Arunachalam Narayanaswamy, Subhashini Venugopalan, Kasumi Widner, Tom Madams, Jorge Cuadros, Ramasamy Kim, Rajiv Raman, Philip C. Nelson, Jessica L. Mega, and Dale R. Webster. Development and Validation of a Deep Learning Algorithm for Detection of Diabetic Retinopathy in Retinal Fundus Photographs. *JAMA*, 316(22):2402–2410, 12 2016. **1**
- [32] Kaiming He, Haoqi Fan, Yuxin Wu, Saining Xie, and Ross Girshick. Momentum contrast for unsupervised visual representation learning. In *Proc. CVPR*, pages 9729–9738, 2020. **2**
- [33] J De Hoog, D Mahapatra, R Garnavi, and F Jalali. Personalized monitoring of injury rehabilitation through mobile device imaging. In *US Patent App. 16/589,046*, 2021. **2**
- [34] He Huang, Changhu Wang, Philip S. Yu, and Chang-Dong Wang. Generative dual adversarial network for generalized zero-shot learning. In *The IEEE Conference on Computer Vision and Pattern Recognition (CVPR)*, pages 801–810, June 2019. **2, 6, 8**
- [35] Jeremy Irvin, Pranav Rajpurkar, Michael Ko, Yifan Yu, Silvana Ciurea-Ilcus, Chris Chute, Henrik Marklund, Behzad Haghgo, Robyn Ball, Katie Shpanskaya, Jayne Seekins, David A. Mong, Safwan S. Halabi, Jesse K. Sandberg, Ricky Jones, David B. Larson, Curtis P. Langlotz, Bhavik N. Patel, Matthew P. Lungren, and Andrew Y. Ng. CheXpert: A large chest radiograph dataset with uncertainty labels and expert comparison. In *arXiv preprint arXiv:1901.07031*, 2017. **1, 5, 6**
- [36] L Ju, X Wang, L Wang, T. Liu, X. Zhao, T. Drummond, D. Mahapatra, and Z. Ge. Relational subsets knowledge distillation for long-tailed retinal diseases recognition. In *arXiv preprint arXiv:2104.11057*, 2021. **2**
- [37] L Ju, X Wang, L Wang, D Mahapatra, X Zhao, M Harandi, T Drummond, Tongliang Liu, and Zongyuan Ge. Improving medical image classification with label noise using dual-uncertainty estimation. In *arXiv preprint arXiv:2103.00528*, 2020. **2**
- [38] Lie Ju, Xin Wang, Lin Wang, Dwarikanath Mahapatra, Xin Zhao, Quan Zhou, Tongliang Liu, and Zongyuan Ge. Improving medical images classification with label noise using dual-uncertainty estimation. *IEEE Transactions on Medical Imaging*, pages 1–1, 2022. **1**
- [39] Lie Ju, Xin Wang, Xin Zhao, Huimin Lu, Dwarikanath Mahapatra, Paul Bonnington, and Zongyuan Ge. Synergic adversarial label learning for grading retinal diseases via knowledge distillation and multi-task learning. *IEEE JBHI*, 100:1–14, 2020. **1**
- [40] Lie Ju, Xin Wang, Xin Zhao, Huimin Lu, Dwarikanath Mahapatra, and Zongyuan Ge. Relational subsets knowledge distillation for long-tailed retinal diseases recognition. In *In MICCAI 2021*, pages 1–11, 2021. **1**
- [41] Kaggle and EyePacs. Kaggle diabetic retinopathy detection. <https://www.kaggle.com/c/diabetic-retinopathy-detection/data>, jul 2015. **6**
- [42] D. Karimi, G. Nir, L. Fazli, P.C. Black, L. Goldenberg, and S.E. Salcudean. Deep learning-based gleason grading of prostate cancer from histopathology images-role of multi-scale decision aggregation and data augmentation. *IEEE J Biomed Health Inform.*, 24(5):1413–1426, 2020. **6**
- [43] Rohit Keshari, Richa Singh, and Mayank Vatsa. Generalized zero-shot learning via over-complete distribution. In *The IEEE Conference on Computer Vision and Pattern Recognition (CVPR)*, pages 13300–13308, June 2020. **2, 6, 8**
- [44] Diederik P. Kingma and Jimmy Ba. Adam: A method for stochastic optimization. In *arXiv preprint arXiv:1412.6980*, 2014. **5**
- [45] Avinash Kori and Ganapathi Krishnamurthi. Zero shot learning for multi-modal real time image registration. In *arXiv preprint arXiv:1908.06213*, 2019. **2**
- [46] S. Kuanar, V. Athitsos, D. Mahapatra, and A. Rajan. Multi-scale deep learning architecture for nucleus detection in renal cell carcinoma microscopy image. In *arXiv preprint arXiv:2104.13557*, 2021. **2**
- [47] S. Kuanar, V Athitsos, D. Mahapatra, K.R. Rao, Z. Akhtar, and D. Dasgupta. Low dose abdominal ct image reconstruction: An unsupervised learning based approach. In *In Proc. IEEE ICIP*, pages 1351–1355, 2019. **1**
- [48] S. Kuanar, D. Mahapatra, V. Athitsos, and K.R. Rao. Gated fusion network for sao filter and inter frame prediction in versatile video coding. In *arXiv preprint arXiv:2105.12229*, 2021. **2**
- [49] Shiba Kuanar, Dwarikanath Mahapatra, Monalisa Bilas, and KR Rao. Multi-path dilated convolution network for haze and glow removal in night time images. *The Visual Computer*, 38(3):1121–1134, 2022. **1**

- [50] S. Kuanar, K.R. Rao, D. Mahapatra, and M. Bilas. Night time haze and glow removal using deep dilated convolutional network. In *arXiv preprint arXiv:1902.00855*, 2019. **2**
- [51] H. Kuang, B. Guthier, M. Saini, D. Mahapatra, and A. El Saddik. A real-time smart assistant for video surveillance through handheld devices. In *In Proc: ACM Intl. Conf. Multimedia*, pages 917–920, 2014. **1**
- [52] Christoph H. Lampert, Hannes Nickisch, and Stefan Harmeling. Attribute-based classification for zero-shot visual object categorization. *IEEE Trans. Pattern Analysis Machine Intelligence*, 36(3):453–465, 2013. **2, 6**
- [53] Kai Li, Martin Renqiang Min, and Yun Fu. Rethinking zero-shot learning: A conditional visual classification perspective. In *CVPR*, pages 3583–3592, 2019. **8**
- [54] Z. Li, D. Mahapatra, J. Tielbeek, J. Stoker, L. van Vliet, and F.M. Vos. Image registration based on autocorrelation of local structure. *IEEE Trans. Med. Imaging*, 35(1):63–75, 2016. **1**
- [55] Yun Liu, Krishna Gadepalli, Mohammad Norouzi, George E. Dahl, Timo Kohlberger, Aleksey Boyko, Subhashini Venugopalan, Aleksei Timofeev, Philip Q. Nelson, Greg S. Corrado, Jason D. Hipp, Lily Peng, and Martin C. Stumpe. Detecting cancer metastases on gigapixel pathology images. In *arXiv preprint arXiv:1703.02442*, 2017. **1**
- [56] Ming Y. Lu, Richard J. Chen, Jingwen Wang, Debora Dillon, and Faisal Mahmood. Semi-supervised histology classification using deep multiple instance learning and contrastive predictive coding. In *arXiv:1910.10825*, 2019. **2**
- [57] D. Mahapatra. Elastic registration of cardiac perfusion images using saliency information. *Sequence and Genome Analysis – Methods and Applications*, pages 351–364, 2011. **1**
- [58] D. Mahapatra. Neonatal brain mri skull stripping using graph cuts and shape priors. In *In Proc: MICCAI workshop on Image Analysis of Human Brain Development (IAHBD)*, 2011. **2**
- [59] Dwarikanath Mahapatra. Registration and segmentation methodology for perfusion mr images: Application to cardiac and renal images. -, pages -, 2011. **1**
- [60] Dwarikanath Mahapatra. Registration and segmentation methodology for perfusion mr images: Application to cardiac and renal images. -, pages -, 2011. **1**
- [61] D. Mahapatra. Cardiac lv and rv segmentation using mutual context information. In *Proc. MICCAI-MLMI*, pages 201–209, 2012. **1**
- [62] D. Mahapatra. Groupwise registration of dynamic cardiac perfusion images using temporal information and segmentation information. In *In Proc: SPIE Medical Imaging*, 2012. **1**
- [63] D. Mahapatra. Landmark detection in cardiac mri using learned local image statistics. In *Proc. MICCAI-Statistical Atlases and Computational Models of the Heart. Imaging and Modelling Challenges (STACOM)*, pages 115–124, 2012. **1**
- [64] D. Mahapatra. Skull stripping of neonatal brain mri: Using prior shape information with graphcuts. *J. Digit. Imaging*, 25(6):802–814, 2012. **1**
- [65] D. Mahapatra. Cardiac image segmentation from cine cardiac mri using graph cuts and shape priors. *J. Digit. Imaging*, 26(4):721–730, 2013. **1**
- [66] D. Mahapatra. Cardiac mri segmentation using mutual context information from left and right ventricle. *J. Digit. Imaging*, 26(5):898–908, 2013. **1**
- [67] D. Mahapatra. Graph cut based automatic prostate segmentation using learned semantic information. In *Proc. IEEE ISBI*, pages 1304–1307, 2013. **1**
- [68] D. Mahapatra. Joint segmentation and groupwise registration of cardiac perfusion images using temporal information. *J. Digit. Imaging*, 26(2):173–182, 2013. **1**
- [69] D. Mahapatra. An automated approach to cardiac rv segmentation from mri using learned semantic information and graph cuts. *J. Digit. Imaging.*, 27(6):794–804, 2014. **1**
- [70] D. Mahapatra. Combining multiple expert annotations using semi-supervised learning and graph cuts for medical image segmentation. *Computer Vision and Image Understanding*, 151(1):114–123, 2016. **1**
- [71] D. Mahapatra. Retinal image quality classification using neurobiological models of the human visual system. In *In Proc. MICCAI-OMIA*, pages 1–8, 2016. **1**
- [72] D. Mahapatra. Consensus based medical image segmentation using semi-supervised learning and graph cuts. In *arXiv preprint arXiv:1612.02166*, 2017. **2**
- [73] D. Mahapatra. Semi-supervised learning and graph cuts for consensus based medical image segmentation. *Pattern Recognition*, 63(1):700–709, 2017. **1**
- [74] D. Mahapatra. Amd severity prediction and explainability using image registration and deep embedded clustering. In *arXiv preprint arXiv:1907.03075*, 2019. **2**
- [75] D. Mahapatra. Generative adversarial networks and domain adaptation for training data independent image registration. In *arXiv preprint arXiv:1910.08593*, 2019. **2**
- [76] D. Mahapatra. Registration of histopathology images using structural information from fine grained feature maps. In *arXiv preprint arXiv:2007.02078*, 2020. **2**
- [77] D. Mahapatra. Interpretability-driven sample selection using self supervised learning for disease classification and segmentation. In *arXiv preprint arXiv:2104.06087*, 2021. **2**
- [78] D. Mahapatra. Learning of inter-label geometric relationships using self-supervised learning: Application to gleason grade segmentation. In *arXiv preprint arXiv:2110.00404*, 2021. **2**
- [79] Dwarikanath Mahapatra. Multimodal generalized zero shot learning for gleason grading using self-supervised learning. In *arXiv preprint arXiv:2111.07646*, 2021. **2**
- [80] D. Mahapatra, K. Agarwal, R. Khosrowabadi, and D.K. Prasad. Recent advances in statistical data and signal analysis: Application to real world diagnostics from medical and biological signals. In *Computational and mathematical methods in medicine*, 2016. **2**
- [81] D. Mahapatra, B. Antony, S. Sedai, and R. Garnavi. Deformable medical image registration using generative adversarial networks. In *In Proc. IEEE ISBI*, pages 1449–1453, 2018. **1**

- [82] D. Mahapatra and B. Bozorgtabar. Retinal vasculature segmentation using local saliency maps and generative adversarial networks for image super resolution. In *arXiv preprint arXiv:1710.04783*, 2017. 2
- [83] D. Mahapatra and B. Bozorgtabar. Progressive generative adversarial networks for medical image super resolution. In *arXiv preprint arXiv:1902.02144*, 2019. 2
- [84] D. Mahapatra, B. Bozorgtabar, and R. Garnavi. Image super-resolution using progressive generative adversarial networks for medical image analysis. *Computerized Medical Imaging and Graphics*, 71:30–39, 2019. 1
- [85] D. Mahapatra, B. Bozorgtabar, and Zongyuan Ge. Medical image classification using generalized zero shot learning. In *In IEEE CVAMD 2021*, pages 3344–3353, 2021. 1
- [86] D. Mahapatra, B. Bozorgtabar, S. Kuanar, and Zongyuan Ge. Self-supervised multimodal generalized zero shot learning for gleason grading. In *In MICCAI-DART 2021*, pages 1–11, 2021. 1
- [87] D. Mahapatra, B. Bozorgtabar, and L. Shao. Pathological retinal region segmentation from oct images using geometric relation based augmentation. In *In Proc. IEEE CVPR*, pages 9611–9620, 2020. 1, 2
- [88] D. Mahapatra, B. Bozorgtabar, J.-P. Thiran, and L. Shao. Pathological retinal region segmentation from oct images using geometric relation based augmentation. In *arXiv preprint arXiv:2003.14119*, 2020. 2
- [89] D. Mahapatra, B. Bozorgtabar, J.-P. Thiran, and L. Shao. Structure preserving stain normalization of histopathology images using self supervised semantic guidance. In *In Proc. MICCAI*, pages 309–319, 2020. 1, 2
- [90] D. Mahapatra, B. Bozorgtabar, J.-P. Thiran, and L. Shao. Structure preserving stain normalization of histopathology images using self supervised semantic guidance. In *arXiv preprint arXiv:2008.02101*, 2020. 2
- [91] D. Mahapatra, S. Bozorgtabar, S. Hewavitahranage, and R. Garnavi. Image super resolution using generative adversarial networks and local saliency maps for retinal image analysis. In *In Proc. MICCAI*, pages 382–390, 2017. 1
- [92] D. Mahapatra, S. Bozorgtabar, J.-P. Thiran, and M. Reyes. Efficient active learning for image classification and segmentation using a sample selection and conditional generative adversarial network. In *In Proc. MICCAI (2)*, pages 580–588, 2018. 1
- [93] D. Mahapatra and J.M. Buhmann. Automatic cardiac rv segmentation using semantic information with graph cuts. In *Proc. IEEE ISBI*, pages 1094–1097, 2013. 1
- [94] D. Mahapatra and J.M. Buhmann. Analyzing training information from random forests for improved image segmentation. *IEEE Trans. Imag. Proc.*, 23(4):1504–1512, 2014. 1
- [95] D. Mahapatra and J.M. Buhmann. Prostate mri segmentation using learned semantic knowledge and graph cuts. *IEEE Trans. Biomed. Engg.*, 61(3):756–764, 2014. 1
- [96] D. Mahapatra and J.M. Buhmann. A field of experts model for optic cup and disc segmentation from retinal fundus images. In *In Proc. IEEE ISBI*, pages 218–221, 2015. 1
- [97] D. Mahapatra and J. Buhmann. Obtaining consensus annotations for retinal image segmentation using random forest and graph cuts. In *In Proc. OMIA*, pages 41–48, 2015. 1
- [98] D. Mahapatra and J. Buhmann. Visual saliency based active learning for prostate mri segmentation. In *In Proc. MLMI*, pages 9–16, 2015. 1
- [99] D. Mahapatra and J. Buhmann. Visual saliency-based active learning for prostate magnetic resonance imaging segmentation. *SPIE Journal of Medical Imaging*, 3(1):014003, 2016. 1
- [100] D. Mahapatra, R. Garnavi, P.K. Roy, and R.B. Tennakoon. System and method to teach and evaluate image grading performance using prior learned expert knowledge base. In *US Patent App. 15/459,457*, 2018. 2
- [101] D. Mahapatra, R. Garnavi, P.K. Roy, and R.B. Tennakoon. System and method to teach and evaluate image grading performance using prior learned expert knowledge base. In *US Patent App. 15/814,590*, 2018. 2
- [102] D. Mahapatra, R. Garnavi, S. Sedai, and P.K. Roy. Joint segmentation and characteristics estimation in medical images. In *US Patent App. 15/234,426*, 2017. 2
- [103] D. Mahapatra, R. Garnavi, S. Sedai, and P.K. Roy. Retinal image quality assessment, error identification and automatic quality correction. In *US Patent 9,779,492*, 2017. 2
- [104] D. Mahapatra, R. Garnavi, S. Sedai, and R.B. Tennakoon. Classification of severity of pathological condition using hybrid image representation. In *US Patent App. 15/426,634*, 2018. 2
- [105] D. Mahapatra, R. Garnavi, S. Sedai, and R.B. Tennakoon. Generating an enriched knowledge base from annotated images. In *US Patent App. 15/429,735*, 2018. 2
- [106] D. Mahapatra, R. Garnavi, S. Sedai, R.B. Tennakoon, and R. Chakravorty. Early prediction of age related macular degeneration by image reconstruction. In *US Patent App. 15/854,984*, 2018. 2
- [107] D. Mahapatra, R. Garnavi, S. Sedai, R.B. Tennakoon, and R. Chakravorty. Early prediction of age related macular degeneration by image reconstruction. In *US Patent 9,943,225*, 2018. 2
- [108] D. Mahapatra and Z. Ge. Combining transfer learning and segmentation information with gans for training data independent image registration. In *arXiv preprint arXiv:1903.10139*, 2019. 2
- [109] D. Mahapatra and Z. Ge. Training data independent image registration with gans using transfer learning and segmentation information. In *In Proc. IEEE ISBI*, pages 709–713, 2019. 1
- [110] D. Mahapatra and Z. Ge. Training data independent image registration using generative adversarial networks and domain adaptation. *Pattern Recognition*, 100:1–14, 2020. 1
- [111] Dwarikanath Mahapatra and Zongyuan Ge. Mr image super resolution by combining feature disentanglement cnns and vision transformers. In -, 2022. 2
- [112] Dwarikanath Mahapatra, Zongyuan Ge, and Mauricio Reyes. Self-supervised generalized zero shot learning for medical image classification using novel interpretable saliency maps. *IEEE Transactions on Medical Imaging*, pages 1–1, 2022. 1

- [113] D. Mahapatra, Z. Ge, and S. Sedai. Joint registration and segmentation of images using deep learning. In *US Patent App. 16/001,566*, 2019. 2
- [114] D. Mahapatra, Z. Ge, S. Sedai, and R. Chakravorty. Joint registration and segmentation of xray images using generative adversarial networks. In *In Proc. MICCAI-MLMI*, pages 73–80, 2018. 1
- [115] D. Mahapatra, S. Gilani, and M.K. Saini. Coherency based spatio-temporal saliency detection for video object segmentation. *IEEE Journal of Selected Topics in Signal Processing.*, 8(3):454–462, 2014. 1
- [116] D. Mahapatra, J.Tielbeek, J.C. Makanyanga, J. Stoker, S.A. Taylor, F.M. Vos, and J.M. Buhmann. Automatic detection and segmentation of crohn’s disease tissues from abdominal mri. *IEEE Trans. Med. Imaging*, 32(12):1232–1248, 2013. 1
- [117] D. Mahapatra, J.Tielbeek, J.C. Makanyanga, J. Stoker, S.A. Taylor, F.M. Vos, and J.M. Buhmann. Active learning based segmentation of crohn’s disease using principles of visual saliency. In *Proc. IEEE ISBI*, pages 226–229, 2014. 1
- [118] D. Mahapatra, J.Tielbeek, J.C. Makanyanga, J. Stoker, S.A. Taylor, F.M. Vos, and J.M. Buhmann. Combining multiple expert annotations using semi-supervised learning and graph cuts for crohn’s disease segmentation. In *In Proc: MICCAI-ABD*, 2014. 1
- [119] D. Mahapatra, J.Tielbeek, F.M. Vos, and J.M. Buhmann. A supervised learning approach for crohn’s disease detection using higher order image statistics and a novel shape asymmetry measure. *J. Digit. Imaging*, 26(5):920–931, 2013. 1
- [120] Dwarikanath Mahapatra, Steven Korevaar, and Ruwan Tenakoon. Gcn based unsupervised domain adaptation with feature disentanglement for medical image classification. In -, 2022. 2
- [121] D. Mahapatra, S. Kuanar, B. Bozorgtabar, and Zongyuan Ge. Self-supervised learning of inter-label geometric relationships for gleason grade segmentation. In *In MICCAI-DART 2021*, pages 57–67, 2021. 1
- [122] D. Mahapatra, Z. Li, F.M. Vos, and J.M. Buhmann. Joint segmentation and groupwise registration of cardiac dce mri using sparse data representations. In *In Proc. IEEE ISBI*, pages 1312–1315, 2015. 1
- [123] Dwarikanath Mahapatra, Alexander Poellinger, Ling Shao, and Mauricio Reyes. Interpretability-driven sample selection using self supervised learning for disease classification and segmentation. *IEEE TMI*, pages 1–15, 2021. 1, 2
- [124] D. Mahapatra, A. Routray, and C. Mishra. An active snake model for classification of extreme emotions. In *IEEE International Conference on Industrial Technology (ICIT)*, pages 2195–2199, 2006. 2
- [125] D. Mahapatra, P.K. Roy, S. Sedai, and R. Garnavi. A cnn based neurobiology inspired approach for retinal image quality assessment. In *In Proc. EMBC*, pages 1304–1307, 2016. 1
- [126] D. Mahapatra, P.K. Roy, S. Sedai, and R. Garnavi. Retinal image quality classification using saliency maps and cnns. In *In Proc. MICCAI-MLMI*, pages 172–179, 2016. 1
- [127] D. Mahapatra, S. Roy, and Y. Sun. Retrieval of mr kidney images by incorporating shape information in histogram of low level features. In *In 13th International Conference on Biomedical Engineering*, pages 661–664, 2009. 2
- [128] D. Mahapatra, S. Saha, A. Vishwanath, and P.R. Bastide. Generating hyperspectral image database by machine learning and mapping of color images to hyperspectral domain. In *US Patent App. 15/949,528*, 2019. 2
- [129] D. Mahapatra and M. Saini. A particle filter framework for object tracking using visual-saliency information. *Intelligent Multimedia Surveillance*, pages 133–147, 2013. 1
- [130] D. Mahapatra, M.K. Saini, and Y. Sun. Illumination invariant tracking in office environments using neurobiology-saliency based particle filter. In *IEEE ICME*, pages 953–956, 2008. 2
- [131] D. Mahapatra, P. Schüffler, J. Tielbeek, F.M. Vos, and J.M. Buhmann. Semi-supervised and active learning for automatic segmentation of crohn’s disease. In *Proc. MICCAI, Part 2*, pages 214–221, 2013. 1
- [132] D. Mahapatra, S. Sedai, and R. Garnavi. Elastic registration of medical images with gans. In *arXiv preprint arXiv:1805.02369*, 2018. 2
- [133] D. Mahapatra, S. Sedai, and K. Halupka. Uncertainty region based image enhancement. In *US Patent App. 10,832,074*, 2020. 2
- [134] D. Mahapatra and A. Singh. Ct image synthesis using weakly supervised segmentation and geometric inter-label relations for covid image analysis. In *arXiv preprint arXiv:2106.10230*, 2021. 2
- [135] D. Mahapatra and Y. Sun. Nonrigid registration of dynamic renal MR images using a saliency based MRF model. In *Proc. MICCAI*, pages 771–779, 2008. 2
- [136] D. Mahapatra and Y. Sun. Registration of dynamic renal mr images using neurobiological model of saliency. In *Proc. ISBI*, pages 1119–1122, 2008. 2
- [137] D. Mahapatra and Y. Sun. Using saliency features for graphcut segmentation of perfusion kidney images. In *In 13th International Conference on Biomedical Engineering*, pages 639–642, 2009. 2
- [138] D. Mahapatra and Y. Sun. Joint registration and segmentation of dynamic cardiac perfusion images using mrf. In *Proc. MICCAI*, pages 493–501, 2010. 2
- [139] D. Mahapatra and Y. Sun. Mrf based joint registration and segmentation of dynamic renal mr images. In *Second International Conference on Digital Image Processing*, volume 7546, pages 285–290, 2010. 2
- [140] D. Mahapatra and Y. Sun. An mrf framework for joint registration and segmentation of natural and perfusion images. In *Proc. IEEE ICIP*, pages 1709–1712, 2010. 2
- [141] D. Mahapatra and Y. Sun. Retrieval of perfusion images using cosegmentation and shape context information. In *Proc. APSIPA Annual Summit and Conference (ASC)*, volume 35, 2010. 2
- [142] D. Mahapatra and Y. Sun. Rigid registration of renal perfusion images using a neurobiology based visual saliency model. *EURASIP Journal on Image and Video Processing.*, pages 1–16, 2010. 1
- [143] D. Mahapatra and Y. Sun. Mrf based intensity invariant elastic registration of cardiac perfusion images us-

- ing saliency information. *IEEE Trans. Biomed. Eng.*, 58(4):991–1000, 2011. 1
- [144] D. Mahapatra and Y. Sun. Orientation histograms as shape priors for left ventricle segmentation using graph cuts. In *In Proc. MICCAI*, pages 420–427, 2011. 2
- [145] D. Mahapatra and Y. Sun. Integrating segmentation information for improved mrf-based elastic image registration. *IEEE Trans. Imag. Proc.*, 21(1):170–183, 2012. 1
- [146] D. Mahapatra, J. Tielbeek, J.M. Buhmann, and F.M. Vos. A supervised learning based approach to detect crohn’s disease in abdominal mr volumes. In *Proc. MICCAI workshop Computational and Clinical Applications in Abdominal Imaging(MICCAI-ABD)*, pages 97–106, 2012. 1
- [147] D. Mahapatra, J. Tielbeek, F.M. Vos, and J.M. Buhmann. Crohn’s disease tissue segmentation from abdominal mri using semantic information and graph cuts. In *Proc. IEEE ISBI*, pages 358–361, 2013. 1
- [148] D. Mahapatra, J. Tielbeek, F.M. Vos, and J.M. Buhmann. Localizing and segmenting crohn’s disease affected regions in abdominal mri using novel context features. In *Proc. SPIE Medical Imaging*, 2013. 1
- [149] D. Mahapatra, J. Tielbeek, F.M. Vos, and J.M. Buhmann. Weakly supervised semantic segmentation of crohn’s disease tissues from abdominal mri. In *Proc. IEEE ISBI*, pages 832–835, 2013. 1
- [150] D. Mahapatra, F.M. Vos, and J.M. Buhmann. Crohn’s disease segmentation from mri using learned image priors. In *In Proc. IEEE ISBI*, pages 625–628, 2015. 1
- [151] D. Mahapatra, F.M. Vos, and J.M. Buhmann. Active learning based segmentation of crohns disease from abdominal mri. *Computer Methods and Programs in Biomedicine*, 128(1):75–85, 2016. 1
- [152] D. Mahapatra, S. Winkler, and S.C. Yen. Motion saliency outweighs other low-level features while watching videos. In *SPIE HVEL.*, pages 1–10, 2008. 2
- [153] Devraj Mandal, Sanath Narayan, Sai Kumar Dwivedi, Vikram Gupta, Shuaib Ahmed, Fahad Shahbaz Khan, and Ling Shao. Out-of-distribution detection for generalized zero-shot action recognition. In *2019 IEEE/CVF Conference on Computer Vision and Pattern Recognition (CVPR)*, pages 9977–9985, 2019. 2
- [154] Quinn McNemar. Note on the sampling error of the difference between correlated proportions or percentages. *Psychometrika*, 12(2):153–157, 1947. 7
- [155] Tomas Mikolov, Kai Chen, Greg Corrado, and Jeffrey Dean. Efficient estimation of word representations in vector space. In *In Proc. ICLR Workshops*, 2013. 2
- [156] Shaobo Min, Hantao Yao, Hongtao Xie, Chaoqun Wang, Zheng-Jun Zha, and Yongdong Zhang. Domain-aware visual bias eliminating for generalized zero-shot learning. In *The IEEE Conference on Computer Vision and Pattern Recognition (CVPR)*, pages 12664–12673, June 2020. 2
- [157] M. Nilsback and A. Zisserman. Automated flower classification over a large number of classes. In *2008 Sixth Indian Conference on Computer Vision, Graphics Image Processing*, pages 722–729, 2008. 6
- [158] Abhineet Pandey, Bhawna Paliwal, Abhinav Dhall, Ramanathan Subramanian, and Dwarikanath Mahapatra. This explains that: Congruent image–report generation for explainable medical image analysis with cyclic generative adversarial networks. In *In MICCAI-iMIMIC 2021*, pages 1–11, 2021. 1
- [159] Genevieve Patterson and James Hays. Sun attribute database: Discovering, annotating, and recognizing scene attributes. In *Proceeding of the 25th Conference on Computer Vision and Pattern Recognition (CVPR)*, 2012. 6
- [160] Akanksha Paul, Narayanan C Krishnan, and Prateek Munjaj. Semantically aligned bias reducing zero shot learning. In *Proceedings of the IEEE Conference on Computer Vision and Pattern Recognition*, pages 7056–7065, 2019. 2
- [161] Hieu H. Pham, Tung T. Le, Dat Q. Tran, Dat T. Ngo, and Ha Q. Nguyen. Interpreting chest x-rays via cnns that exploit hierarchical disease dependencies and uncertainty labels. In *arXiv preprint arXiv:1911.06475.*, 2020. 6
- [162] P. Rajpurkar, J. Irvin, K. Zhu, B. Yang, H. Mehta, T. Duan, D. Ding, A. Bagul, C. Langlotz, K. Shpanskaya, M. P Lungren, and A.Y Ng. Chexnet: Radiologist-level pneumonia detection on chest x-rays with deep learning. In *arXiv preprint arXiv:1711.05225.*, 2017. 5
- [163] P. Roy, R. Chakravorty, S. Sedai, D. Mahapatra, and R. Garnavi. Automatic eye type detection in retinal fundus image using fusion of transfer learning and anatomical features. In *In Proc. DICTA*, pages 1–7, 2016. 1
- [164] P.K. Roy, D. Mahapatra, R. Garnavi, and R.B. Tennakoon. System and method to teach and evaluate image grading performance using prior learned expert knowledge base. In *US Patent App. 10,984,674*, 2021. 2
- [165] P. Roy, R. Tennakoon, K. Cao, S. Sedai, D. Mahapatra, S. Maetschke, and R. Garnavi. A novel hybrid approach for severity assessment of diabetic retinopathy in colour fundus images,. In *In Proc. IEEE ISBI*, pages 1078–1082, 2017. 1
- [166] M. Saini, B. Guthier, H. Kuang, D. Mahapatra, and A.E. Saddik. szoom: A framework for automatic zoom into high resolution surveillance videos. In *arXiv preprint arXiv:1909.10164*, 2019. 2
- [167] Kuniaki Saito, Donghyun Kim, Stan Sclaroff, and Kate Saenko. Universal domain adaptation through self supervision. In *In Proc. NeurIPS*, 2020. 2
- [168] P. Schüffler, D. Mahapatra, J. Tielbeek, F.M. Vos, J. Makanyanga, D.A. Pends, C.Y. Nio, J. Stoker, S.A. Taylor, and J.M. Buhmann. A model development pipeline for crohns disease severity assessment from magnetic resonance images. In *In Proc. MICCAI-ABD*, 2013. 1
- [169] P. Schüffler, D. Mahapatra, J. Tielbeek, F.M. Vos, J. Makanyanga, D.A. Pends, C.Y. Nio, J. Stoker, S.A. Taylor, and J.M. Buhmann. Semi automatic crohns disease severity assessment on mr imaging. In *In Proc. MICCAI-ABD*, 2014. 1
- [170] Edgar Schonfeld, Sayna Ebrahimi, Samarth Sinha, Trevor Darrell, and Zeynep Akata. Generalized zero-and few-shot learning via aligned variational autoencoders. In *In Proc. IEEE CVPR*, pages 8247–8255, 2019. 2
- [171] Peter J Schüffler, Dwarikanath Mahapatra, Franciscus M Vos, and Joachim M Buhmann. Computer aided crohn’s

- disease severity assessment in mri. In *VIGOR++ Workshop 2014-Showcase of Research Outcomes and Future Outlook*, pages –, 2014. [1](#)
- [172] S. Sedai, D. Mahapatra, B. Antony, and R. Garnavi. Joint segmentation and uncertainty visualization of retinal layers in optical coherence tomography images using bayesian deep learning. In *In Proc. MICCAI-OMIA*, pages 219–227, 2018. [1](#)
- [173] S. Sedai, D. Mahapatra, Z. Ge, R. Chakravorty, and R. Garnavi. Deep multiscale convolutional feature learning for weakly supervised localization of chest pathologies in x-ray images. In *In Proc. MICCAI-MLMI*, pages 267–275, 2018. [1](#)
- [174] S. Sedai, D. Mahapatra, S. Hewavitharanage, S. Maetschke, and R. Garnavi. Semi-supervised segmentation of optic cup in retinal fundus images using variational autoencoder,. In *In Proc. MICCAI*, pages 75–82, 2017. [1](#)
- [175] S. Sedai, P.K. Roy, D. Mahapatra, and R. Garnavi. Segmentation of optic disc and optic cup in retinal fundus images using shape regression. In *In Proc. EMBC*, pages 3260–3264, 2016. [1](#)
- [176] S. Sedai, P.K. Roy, D. Mahapatra, and R. Garnavi. Segmentation of optic disc and optic cup in retinal images using coupled shape regression. In *In Proc. MICCAI-OMIA*, pages 1–8, 2016. [1](#)
- [177] Shikhar Srivastava, Mohammad Yaqub, Karthik Nandakumar, Zongyuan Ge, and Dwarikanath Mahapatra. Continual domain incremental learning for chest x-ray classification in low-resource clinical settings. In *In MICCAI-FAIR 2021*, pages 1–11, 2021. [1](#)
- [178] Hidenori Takahashi, Hironobu Tampo, Yusuke Arai, Yuji Inoue, and Hidetoshi Kawashima. Applying artificial intelligence to disease staging: Deep learning for improved staging of diabetic retinopathy. *Plos One*, 12(6), 2017. [6](#)
- [179] R. Tennakoon, D. Mahapatra, P. Roy, S. Sedai, and R. Garnavi. Image quality classification for dr screening using convolutional neural networks. In *In Proc. MICCAI-OMIA*, pages 113–120, 2016. [1](#)
- [180] J. Tong, D. Mahapatra, P. Bonnington, T. Drummond, and Z. Ge. Registration of histopathology images using self supervised fine grained feature maps. In *In Proc. MICCAI-DART Workshop*, pages 41–51, 2020. [1](#), [2](#)
- [181] Ruchika Verma, Neeraj Kumar, Abhijeet Patil, Nikhil Cherian Kurian, Swapnil Rane, Simon Graham, Quoc Dang Vu, Mieke Zwager, Shan E. Ahmed Raza, Nasir Rajpoot, Xiyi Wu, Huai Chen, Yijie Huang, Lisheng Wang, Hyun Jung, G. Thomas Brown, Yanling Liu, Shuolin Liu, Seyed Alireza Fatemi Jahromi, Ali Asghar Khani, Ehsan Montahaei, Mahdiah Soleymani Baghshah, Hamid Behroozi, Pavel Semkin, Alexandr Rassadin, Prasad Dutande, Romil Lodaya, Ujjwal Baid, Bhakti Baheti, Sanjay Talbar, Amirreza Mahbod, Rupert Ecker, Isabella Ellinger, Zhipeng Luo, Bin Dong, Zhengyu Xu, Yuehan Yao, Shuai Lv, Ming Feng, Kele Xu, Hasib Zunair, Abdessamad Ben Hamza, Steven Smiley, Tang-Kai Yin, Qi-Rui Fang, Shikhar Srivastava, Dwarikanath Mahapatra, Lubomira Trnavska, Hanyun Zhang, Priya Lakshmi Narayanan, Justin Law, Yinyin Yuan, Abhiroop Tejomay, Aditya Mitkari, Dinesh Koka, Vikas Ramachandra, Lata Kini, and Amit Sethi. Monusac2020: A multi-organ nuclei segmentation and classification challenge. *IEEE Transactions on Medical Imaging*, 40(12):3413–3423, 2021. [1](#)
- [182] Vinay Kumar Verma, Gundeep Arora, Ashish Mishra, and Piyush Rai. Generalized zero-shot learning via synthesized examples. In *The IEEE Conference on Computer Vision and Pattern Recognition (CVPR)*, pages 4281–4289, 2018. [1](#), [2](#)
- [183] F. M. Vos, J. Tielbeek, R. Naziroglu, Z. Li, P. Schüffler, D. Mahapatra, Alexander Wiebel, C. Lavini, J. Buhmann, H. Hege, J. Stoker, and L. van Vliet. Computational modeling for assessment of IBD: to be or not to be? In *Proc. IEEE EMBC*, pages 3974–3977, 2012. [1](#)
- [184] C. Wah, S. Branson, P. Welinder, P. Perona, and S. Belongie. The Caltech-UCSD Birds-200-2011 Dataset. Technical Report CNS-TR-2011-001, California Institute of Technology, 2011. [6](#)
- [185] X. Wang, Y. Peng, L. Lu, Z. Lu, M. Bagheri, and R.M. Summers. Chestx-ray8: Hospital-scale chest x-ray database and benchmarks on weakly-supervised classification and localization of common thorax diseases. In *In Proc. CVPR*, 2017. [1](#), [5](#), [6](#)
- [186] Jiamin Wu, Tianzhu Zhang, Zheng-Jun Zha, Jiebo Luo, Yongdong Zhang, and Feng Wu. Self-supervised domain-aware generative network for generalized zero-shot learning. In *The IEEE Conference on Computer Vision and Pattern Recognition (CVPR)*, pages 12767–12776, June 2020. [2](#), [6](#), [7](#), [8](#)
- [187] Zhirong Wu, Yuanjun Xiong, Stella X. Yu, and Dahua Lin. Unsupervised feature learning via non-parametric instance discrimination. In *2018 IEEE/CVF Conference on Computer Vision and Pattern Recognition*, pages 3733–3742, 2018. [3](#)
- [188] Yongqin Xian, Christoph H. Lampert, Bernt Schiele, and Zeynep Akata. Zero-shot learning a comprehensive evaluation of the good, the bad and the ugly. *IEEE Trans. Pattern Analysis Machine Intelligence*, 41(9):2251–2265, 2018. [1](#), [2](#), [5](#), [6](#)
- [189] Yongqin Xian, Tobias Lorenz, Bernt Schiele, and Zeynep Akata. Feature generating networks for zero-shot learning. In *In Proc. IEEE CVPR*, pages 5542–5551, 2018. [1](#), [2](#)
- [190] Yongqin Xian, Saurabh Sharma, Bernt Schiele, and Zeynep Akata. f-vaegan-d2: A feature generating framework for any-shot learning. In *The IEEE Conference on Computer Vision and Pattern Recognition (CVPR)*, pages 10275–10284, June 2019. [1](#), [2](#), [8](#)
- [191] Y. Xing, Z. Ge, R. Zeng, D. Mahapatra, J. Seah, M. Law, and T. Drummond. Adversarial pulmonary pathology translation for pairwise chest x-ray data augmentation. In *In Proc. MICCAI*, pages 757–765, 2019. [1](#)
- [192] J. Zilly, J. Buhmann, and D. Mahapatra. Boosting convolutional filters with entropy sampling for optic cup and disc image segmentation from fundus images. In *In Proc. MLMI*, pages 136–143, 2015. [1](#)

- [193] J. Zilly, J.M. Buhmann, and D. Mahapatra. Glaucoma detection using entropy sampling and ensemble learning for automatic optic cup and disc segmentation. *In Press Computerized Medical Imaging and Graphics*, 55(1):28–41, 2017. [1](#)